BROWNIAN DYNAMICS SIMULATION OF RESTRICTED ROTATIONAL DIFFUSION

M. CARMEN LÓPEZ MARTÍNEZ AND JOSÉ GARCÍA DE LA TORRE
Departamento de Química Física, Facultad de Ciencias Químicas y Matemáticas, Universidad de Murcia, 30001 Murcia, Spain

ABSTRACT The restricted rotational diffusion of an axially symmetric particle is simulated by the Brownian dynamics technique. In addition to the wobbling-in-a-cone model, several continuous potentials are considered. The particle studied is particularly simple: a sphere anchored to a point fixed in space. However, presenting the results in a convenient, reduced form, they are valid for any axially symmetric particle. From simulated rotational trajectories, we calculate $\langle P_2(\cos\alpha)\rangle$ as a function of t, where α is the angle between two orientations separated by time t and P_2 is the second Legendre polynomial. This correlation function is closely related to time-resolved electro-optic and spectroscopic properties. Simulated results for the cone model are in excellent agreement with the quasiexact results of Lipari and Szabo (1981, *J. Chem. Phys.*, 75:2971–2976). Thus we confirm the good performance of the simulation technique and the validity of our working conditions. Novel results are presented for continuous restricting potentials, $V(\theta)$. The $\langle P_2\rangle$ results for $V = \frac{1}{2}K\theta^2$ and $V = Q(1 - \cos\theta)$ are practically the same if K and Q are chosen so that the long-time $\langle P_2\rangle$ values coincide. Thus, the quadratic potential seems to be a good representation of any monotonically increasing potential. However, for an uniaxial potential such as $V = C\sin^2\theta$, the decay is appreciably faster. The $\langle P_2\rangle$ decays simulated for the continuous potentials are analyzed by the monoexponential version of the cone model. We found that such an analysis produces an overestimation of the true rotational diffusion coefficient of ~15% only, although for uniaxial potentials the error may be larger.

INTRODUCTION

The rotational diffusivity of biological macromolecules or particles freely suspended in a fluid is an excellent source of information on their size and shape. This information can be extracted from frequency- or time-resolved electro-optic and spectroscopic properties using theories that are now well developed (1–4). However, there are cases of great relevance in which rotational diffusion is restricted by the immediate surroundings of the diffusing entity. Such happens when the rotational diffusion takes place in a membrane (5, 6). Another example is the rotation of a part or subunit of a segmentally flexible macromolecule, like the S1 subfragment of myosin in free myosin or in filaments (7, 8), or a quite small residue flexibly attached to the surface of a globular macromolecule (9, 10).

In a pioneering work, Kinosita et al. (11) presented numerical results for the wobbling-in-a-cone model, in which rotational diffusion is assumed to be free within a cone of semiangle θ_0 and forbidden on the outside. Lipari and Szabo (12) obtained a closed-form, approximate result for the correlation function $\langle P_2(\cos\alpha)\rangle$, where P_2 is the second Legendre polynomial and α is the angle between two successive orientations, separated by time t, of the long axis of the particle. Their monoexponential approximation is particularly useful in practice because of its simplicity. Later the same authors (13) presented a more accurate, multiexponential expression for that correlation function. The wobbling-in-a-cone or, shortly, cone model has been further developed in recent years (14, 15).

Apart from the accuracy of its solution, the cone model seems a strong oversimplification of the real potential energy of the particle in the orienting environment. If, in a case different from those cited above, the restriction to rotation were caused by an external field, the cone model is clearly inappropriate. Szabo (14) has suggested guidelines to introduce continuous potentials, $V(\theta)$, but the only numerical results we are aware of are those reported by Kinosita et al. (16) for a quadratic potential, $V(\theta) = \frac{1}{2}K\theta^2$. These results are based on monoexponential approximate solutions, whose validity should be examined.

Previous theoretical works (11–16) were based in the differential equation for rotational diffusion, whose analytic or numeric handling presented some problems. Thus, Kinosita et al. (16) were unable to obtain numerical results for the $\frac{1}{2}K\theta^2$ potential for high values of K. In this work we propose the use of an essentially different approach, the Brownian dynamics simulation technique, which is based on the statistics of the diffusion process. To our knowledge, the only antecedents in simulation of rotational diffusion are the works by Harvey and Cheung, who used a somewhat primitive procedure for the free rotation of rigid (17)

Correspondence should be addressed to Dr. de la Torre.

and segmentally flexible (18) macromolecules. In this work we use the robust and efficient algorithm of Ermak and McCammon (19), adapted here for rotational motion by a suitable model. This algorithm has been proved to be useful not only for obtaining instantaneous values of the rotational coefficients (20) but also to calculate rotational correlation functions of rigid and semiflexible macromolecules (21–23; Díaz, F.G., A. Iniesta, and J. García de la Torre, manuscript in preparation). In this paper we show that it can be easily extended to simulate rotational diffusion under continuous or discontinuous potentials.

We first simulate the $\langle P_2 \rangle$ function for the wobbling-in-a-cone model. The comparison of the simulated results with those from a quasiexact expression gives confidence in the accuracy of the simulation procedure and the working conditions. We next study the effect on rotational diffusion (concretely, in the decay of $\langle P_2 \rangle$) of continuous potentials of varying strength. Mimicking the usual treatment of experimental data, the simulated results are analyzed in terms of the Lipari–Szabo (12) monoexponential version of the cone model, obtaining an effective decay rate that is compared with the true one. In this way we can establish the adequacy of this widely used version of the cone model to represent more realistic potentials. We wish to anticipate here that the performance of the monoexponential treatment is rather good.

From another point of view, our work illustrates the simplicity of the Brownian dynamics simulation techniques in the study of rotational diffusion under arbitrarily complex conditions.

THEORY AND METHODS

Models

We shall assume that rotational reorientation is restricted by a potential $V(\theta)$, where θ is the angle made by the particle's axis and certain laboratory-fixed axis, Z. We have a simple example in the cone model, in which rotation is free within a cone of semiangle θ_0 and forbidden outside. The potential is

$$V(\theta) = \begin{cases} 0 \text{ if } \theta \leq \theta_0 \\ \infty \text{ if } \theta > \theta_0 \end{cases}. \quad (1)$$

The cone model is a strong oversimplification of any real potential. In any case, $V(\theta)$ can be expanded in Taylor series,

$$V(\theta) = V(0) + (\mathrm{d}V/\mathrm{d}\theta)_0\theta + \tfrac{1}{2}(\mathrm{d}^2V/\mathrm{d}\theta^2)_0\theta^2 + \mathcal{O}(\theta^3). \quad (2)$$

The laboratory-fixed axis used to measure θ can be taken such that it coincides with the equilibrium orientation, so that $(\mathrm{d}V/\mathrm{d}\theta)_0 = 0$. Taking for convenience $V(0) = 0$, and neglecting third-order and higher terms, we are left with

$$V/k_BT = \tfrac{1}{2}K\theta^2, \quad (3)$$

where

$$K = (1/k_BT)(\mathrm{d}^2V/\mathrm{d}\theta^2)_0, \quad (4)$$

and k_BT is the Boltzmann factor. The quadratic potential of Eq. 3 may be inadequate for moderate or high θ. It is advisable to study rotational diffusion under more realistic potentials. For instance, if the particle has a dipole moment aligned with its symmetry axis, and an electric field is applied along Z, the potential is of the form

$$V/k_BT = Q(1 - \cos\theta). \quad (5)$$

These potentials are not symmetric in the $\theta \rightarrow \pi - \theta$ transformation. In contrast, such symmetry is expected in uniaxial systems (cylindrical probes in bilayers, for instance). A plausible symmetric potential is

$$V/k_BT = C\sin^2\theta. \quad (6)$$

This is also the potential for an apolar particle with a cylindrically symmetric polarizability in an electric field.

The equilibrium orientational distribution function, $p(\theta)$, contains the Boltzmann exponential and a $\sin\theta$ geometrical weight. In normalized form, it is given by

$$p(\theta) = \sin\theta \exp[-V(\theta)/k_BT] / \int_0^\pi \mathrm{d}\theta \sin\theta \exp[-V(\theta)/k_BT]. \quad (7)$$

Eq. 7 can be used to calculate the equilibrium average of any orientation-dependent quantity. For instance,

$$\langle \cos^2\theta \rangle = \int_0^\pi \mathrm{d}\theta \cos^2\theta p(\theta). \quad (8)$$

In the cone model, Eqs. 7 and 8 reduce to (12)

$$p(\theta) = \begin{cases} [2\pi(1 - \cos\theta_0)]^{-1} & \text{if} \quad \theta \leq \theta_0 \\ 0 & \text{if} \quad \theta > \theta_0 \end{cases}, \quad (9)$$

and

$$\langle \cos^2\theta \rangle = [1 + \cos\theta_0(1 + \cos\theta_0)]/3. \quad (10)$$

For other potentials the integrals in Eqs. 7 and 8 can be evaluated numerically. In Table I we present values for $\langle \cos^2\theta \rangle$ for the cone model with various choices of θ_0. Since it is desirable to compare models with the same $\langle \cos^2\theta \rangle$ values, we give in Table I the values of the constants in Eqs. 3, 5, and 6 that yield the same average. The four model potentials and the associated $p(\theta)$ functions are displayed in Fig. 1 for cases having a common value of $\langle \cos^2\theta \rangle = 0.736$ corresponding to the cone model with $\theta_0 = 45°$.

Besides the obvious difference between the aspect of the functions for the cone model and that for the other, continuous potentials, we note the difference between the quadratic and cosine potentials, on the one hand, and the symmetric squared-sine potential, on the other. At low angles, $V(\theta)$ is nearly the same for all the continuous

TABLE I
RESULTS FOR $\langle\cos^2\theta\rangle$ AND RELATED QUANTITIES FOR THE CONE MODEL, AND VALUES OF THE CONSTANTS IN OTHER POTENTIALS THAT GIVE THE SAME RESULTS

Cone model				Constants for other potentials		
θ_0	$\langle\cos^2\theta\rangle$	S	$\langle P_2\rangle_\infty$	K(Eq. 3)	Q(Eq. 5)	C(Eq. 6)
20	0.941	0.911	0.831	32.2	32.8	17.5
30	0.872	0.808	0.653	13.9	14.5	8.54
45	0.736	0.604	0.365	5.77	6.39	4.49
66.4	0.520	0.280	0.078	2.17	2.62	1.89

models, because, as $(dV/d\theta)_{\theta=0} = 0$ for all of them, the potential is always quadratic at θ close to zero. The quadratic potential and the cosine potential deviate from each other at higher θ, but the deviation is unimportant because the Boltzmann exponential is nearly zero in any case. Indeed, we see that $p(\theta)$ is practically the same for the two potentials, and we therefore hope to obtain very similar results from them. This will be confirmed later in our calculations of the orientational correlation function. Extrapolating this situation, we expect that results for monotonically increasing potentials with $(dV/d\theta)_{\theta=0} = 0$ will be quite close to those of the quadratic potential.

The squared-sine potential has a hill at $\theta = 90°$, $(V/kT = C)$. There is a finite probability for crossing the hill that increases with decreasing values of C. Apparently, this should produce an increase in the rotational diffusion rate.

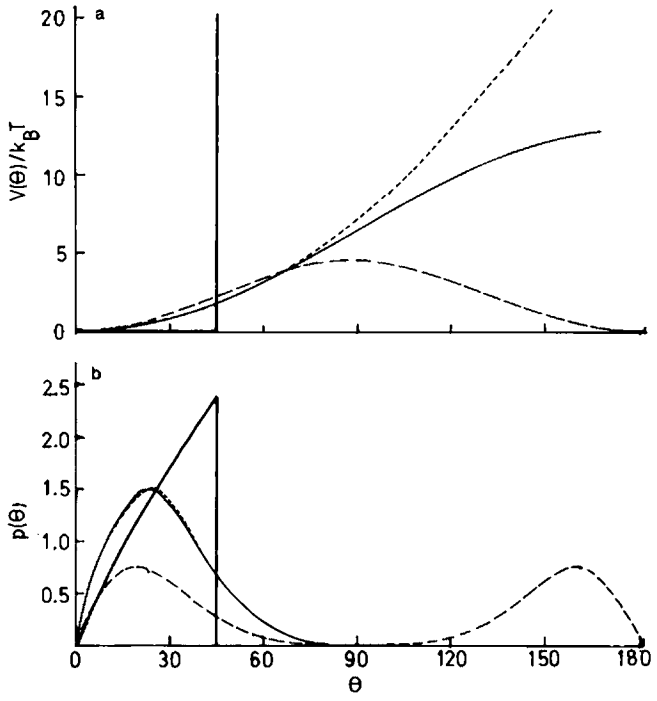

FIGURE 1 (*a*) Potential energy in units of k_BT vs. θ for several models (—), cone model with $\theta_0 = 45°$; (----) elastic potential (Eq. 3) with $K = 5.77$; (—) cosine potential (Eq. 5) with $Q = 6.39$; (– – –) squared-sine potential (Eq. 6) with $C = 4.49$. In all cases $\langle\cos^2\theta\rangle = 0.736$ (see Table I). (*b*) Orientational distribution functions at equilibrium, $p(\theta)$ in the same cases.

Rotational Relaxation

We are concerned with the diffusive reorientation of the symmetry axis of an axially symmetric particle. The corresponding rotational diffusion coefficient is denoted as $D_\perp$. It is evident that if time, t', is expressed in the reduced, dimensionless form

$$t = D_\perp t', \tag{11}$$

then the variation of orientation-dependent properties with t will be independent of $D_\perp$. In other words, if the theoretical or simulation results are presented in terms of t, they will be valid for an arbitrary, axially symmetric particle.

The reorientational relaxation can be expressed in terms of the correlation function of the second Legendre polynomial of the cosine of the angle subtended by two orientations at instants separated by time t'

$$\langle P_2\rangle \equiv \langle P_2[\mathbf{u}(\tau)\cdot\mathbf{u}(\tau+t')]\rangle_\tau$$
$$= \lim_{T\to\infty}(1/T)\int_0^T P_2[\mathbf{u}(\tau)\cdot\mathbf{u}(\tau+t')]d\tau, \tag{12}$$

where $\mathbf{u}$ is a unit vector along the particle's axis and $P_2(x) = (3x^2 - 1)/2$. For unrestricted rotational relaxation of the axially symmetric particle we have the known result

$$\langle P_2(t')\rangle = e^{-6D_\perp t'} = e^{-6t}. \tag{13}$$

If rotational diffusion is restricted, the decay of $\langle P_2\rangle$ is no longer a single exponential, and its infinite-time value, $\langle P_2\rangle_\infty$ is not zero. Instead, we have

$$\langle P_2\rangle_\infty = S^2, \tag{14}$$

where S is the so-called order parameter, given by

$$S = \langle P_2(\cos\theta)\rangle = (3\langle\cos^2\theta\rangle - 1)/2. \tag{15}$$

Values of S and $\langle P_2\rangle_\infty$ for several values of θ_0 and the corresponding constants of the continuous potentials are given in Table I.

The $\langle P_2\rangle$ function is closely related to the decay of optical or spectroscopic properties. Thus, if either the absorption dipole or the emission dipole of the particle are aligned with its symmetry axis, $\langle P_2\rangle$ coincides with the decay of fluorescence or phosphorescence anisotropy, $r(t)$, normalized to the zero-time value, i.e., $\langle P_2\rangle = r(t)/r(0)$, so that $\langle P_2\rangle_\infty = r(\infty)/r(0)$.

We now summarize previous studies on $\langle P_2\rangle$ for restricted rotational diffusion. In their pioneering work, Kinosita et al. (11) proposed the cone model and found an approximate monoexponential solution of the type

$$\langle P_2\rangle = (1 - \langle P_2\rangle_\infty)e^{-t/\text{reff}} + \langle P_2\rangle_\infty, \tag{16}$$

where τ_{eff} is an effective relaxation time, which depends solely on the parameter θ_0 (recall that we are expressing times t and τ_{eff} in units of $1/D_\perp$). Lipari and Szabo (12) proposed to obtain τ_{eff} by requiring that the area under the approximate $\langle P_2 \rangle$ and the exact one must be the same. The result is Eq. 24 in reference 12. Later, Lipari and Szabo (13) obtained an improved triexponential function

$$\langle P_2 \rangle = \sum_{k=0}^{2} G_k \exp(-t/\tau_k), \tag{17}$$

where the G_k and τ_k are given by Eqs. 2.5 and 2.7 of their paper. Comparing their results with numerical results of Kinosita et al. (11), Lipari and Szabo (13) found that Eq. 17 is virtually exact for a θ_0 as large as 66°. Kinosita et al. (16) have later tackled the case of the quadratic potential of Eq. 3, assuming an approximate monoexponential solution of the type of Eq. 16. We finally recall that a comprehensive formalism for restricted rotational diffusion has been more recently presented by Szabo (14). Concretely, he derived a multiexponential approximation for $\langle P_2 \rangle$ in the case of potentials that are symmetric ~90°. The complexity of his general formalism and the mentioned approximation is remarkable.

Brownian Dynamics Simulation

Since the variation of $\langle P_2 \rangle$ with reduced time t does not depend on the actual value of $D_\perp$ and is therefore the same for any cylindrically symmetric particle, we have chosen a very simple particle for the simulations. It consists of a single sphere of radius a tethered to a point fixed in space, which is taken as the origin of a Cartesian axes, by a frictionless, stiff spring (see Fig. 2). The elastic potential for the spring is quadratic; in a dimensionless form we can write

$$(k_B T)^{-1}\phi(r) = (\tfrac{1}{2}\delta^2)(\ell - r')^2, \tag{18}$$

where r' is the instantaneous distance from the origin to the center of the sphere, ℓ, is the equilibrium value of r' and δ is a spring constant (note that $\Delta r' \equiv (\langle r'^2 \rangle - \langle r' \rangle^2)^{1/2} \simeq \delta$ for low δ).

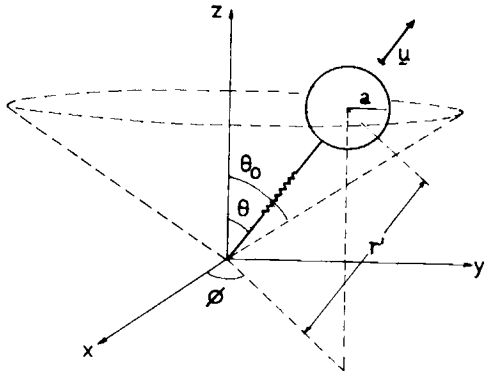

FIGURE 2 Model particle used in the simulation.

The translational diffusion coefficient of the sphere is $D_t = k_B T/f_t$ where f_t is the translational friction coefficient of the sphere. From elementary hydrodynamics we know that the rotational friction coefficient for perpendicular rotation is $f_r = \ell^2 f_t$, and therefore the rotational diffusion coefficient, obtained as $D = k_B T/f_r$, is given by

$$D = D_t/\ell^2. \tag{19}$$

Rigorously, $\langle r'^2 \rangle$ should appear instead of ℓ^2 in Eq. 19. However, we use values of δ small enough so that $\langle r'^2 \rangle \simeq \ell^2$. In Eq. 19 we have neglected the so-called volume correction (24), and it is therefore valid if a is appreciably smaller than ℓ. Fortunately, this assumption can be made without any loss of generality because the results in terms of the reduced time t do not depend on the actual value of a.

If there is a potential associated with θ, of the form of one of the Eqs. 3, 5, or 6, the total potential will be $V_{tot} = V(\theta) + \phi(r')$. The total force acting on the sphere, $\mathbf{F}'_{tot} = -\nabla V_{tot}$, can be split into two contributions, $\mathbf{F}'_{tot} = \mathbf{F}'_r + \mathbf{F}'_\theta$ given by

$$\mathbf{F}_r = (\ell/k_B T)\mathbf{F}'_r = [(1 - r)/\delta^2]\mathbf{u}, \tag{20}$$

and

$$\mathbf{F}_\theta = (\ell/k_B T)\mathbf{F}'_\theta = F_{\theta,x}\mathbf{e}_x + F_{\theta,y}\mathbf{e}_y + F_{\theta,z}\mathbf{e}_z, \tag{21}$$

with

$$\begin{aligned} F_{\theta,x} &= -|\mathbf{F}_\theta|\cos\theta\cos\phi \\ F_{\theta,y} &= -|\mathbf{F}_\theta|\cos\theta\sin\phi \\ F_{\theta,z} &= |\mathbf{F}_\theta|\sin\theta, \end{aligned} \tag{22}$$

and

$$|\mathbf{F}_\theta| = \left(\frac{k_B T}{\ell}\right)\frac{1}{r}\frac{dV}{d\theta}. \tag{23}$$

In Eq. 20, $\mathbf{u} = \mathbf{r}'/r'$ and

$$r = r'/\ell. \tag{24}$$

Note that we are using unprimed symbols for reduced, dimensionless quantities: t is expressed in units of $D_\perp^{-1}$, r in units of ℓ, and the F is in units of $k_B T/\ell$.

The Brownian dynamics of the tethered sphere must obey a Langevin equation:

$$f_t \frac{d\mathbf{r}'}{dt'} = \mathbf{F}'_{tot}(r', \theta) + \mathbf{L}(t'), \tag{25}$$

in which the inertial term has been neglected, $\mathbf{F}'_{tot}$ is the already described force due to V_{tot} and $\mathbf{L}(t')$ is a Langevin stochastic force. An algorithmic solution of Eq. 25 is

$$\mathbf{r}' = \mathbf{r}'_0 + (\Delta t'/k_B T)D_t\mathbf{F}'_{tot} + R'. \tag{26}$$

$\mathbf{r}'_0$ is the position vector of the sphere at some instant t', and r' is the position vector after a time step $\Delta t'$. $\mathbf{R}'$ is a random

vector with Gaussian-like distributed coordinates having zero mean and variance $\langle R_\alpha'^2 \rangle = 2D_t\Delta t'$. We note that Eq. 26 is a particularization for a single sphere of the Ermak–McCammon equation (19).

It is useful to rewrite Eq. 26 in terms of reduced quantities. If $\mathbf{R} = \mathbf{R}'/\ell$ and $\Delta t = D_\perp \Delta t'$, we arrive at

$$\mathbf{r} = \mathbf{r}_0 + \Delta t(\mathbf{F}_r + \mathbf{F}_\theta) + \mathbf{R}, \tag{27}$$

in which F_{tot} has been written more explicitly. The statistical properties of $\mathbf{R}$ are

$$\left.\begin{aligned} \langle R_\alpha \rangle &= 0 \\ \langle R_\alpha^2 \rangle &= 2\Delta t \\ \langle R_\alpha R_\beta \rangle &= 0 \end{aligned}\right\} \qquad \alpha,\beta = x,y,z \qquad \alpha \neq \beta. \tag{28}$$

In Eq. 28 (or Eq. 26) it is implicit that the time step Δt is small enough so that the forces do not vary appreciably along the resulting displacement $\mathbf{r} - \mathbf{r}_0$ (19).

Eqs. 27 and 28 are the basis for our Brownian dynamics simulation procedure. The repetitive application of Eq. 27, taking the final position of a step as the initial position of the next one, gives a time series of $\mathbf{r}$ values or, in other words, a trajectory of the particle. If the number of steps is n, the length of the trajectory is $T = n\Delta t$. At each step we evaluate the forces F_θ and F_r using Eqs. 20–23 in which r and θ are set equal to the initial values, r_0 and θ_i. The Gaussian-like distributed random values of R_α with zero mean and variance $2\Delta t$ are obtained as

$$R_\alpha = \sqrt{2\Delta t}\left(-6 + \sum_{m=1}^{12} a_m\right), \tag{29}$$

where the a_m are twelve random numbers with uniform distribution in (0, 1) (25).

In the specific case of the cone model we set $F_\theta = 0$ for free diffusion within the cone. Final values of θ are allowed if $\theta \leq \theta_0$. If $\theta > \theta_0$ the values of r and ϕ that resulted in the step are regarded as valid, but θ is corrected to a new value θ_f because along the θ displacement, $\Delta\theta = \theta - \theta_i$, the particle crossed the "wall" of the cone. The first part of the increment $\Delta_1\theta = \theta_0 - \theta_i$ is allowed. At θ_0 the particle bounces on the wall, and the remaining of the displacement $\Delta_2\theta = \theta - \theta_0$ takes place inward, so that the final position is $\theta_f = \theta_i + \Delta_1\theta - \Delta_2\theta$, or $\theta_f = 2\theta_0 - \theta$. With the resulting r, θ_f, and ϕ, the coordinates of the particle are calculated and used for the next step.

The values of $\mathbf{u}$ as a function of t are then used to compute the correlation function $\langle P_2 \rangle$, using a discrete form of Eq. 12 (22)

$$\langle P_2 \rangle_j = [1/(n - j + 1)] \sum_{k=0}^{n-j} P_2(k, j + k), \tag{30}$$

where $\langle P_2 \rangle_j$ is the value of the correlation function at time $j\Delta t$ and

$$P_2(k, j + k) \equiv P_2[\mathbf{u}(k\Delta t) \cdot \mathbf{u}[(j + k)\Delta t]]. \tag{31}$$

RESULTS AND DISCUSSION

In typical runs trajectories with $n = 500{,}000$ steps were simulated. The values assigned to the time step Δt were 5×10^{-4}, 6×10^{-4}, 8×10^{-4}, 1×10^{-3}, for $\theta_0 = 20°$, 30°, 45°, and 66.4°, respectively. For other potentials Δt was the same as for the equivalent θ_0 in the cone model. From the recorded trajectories, the correlation function was evaluated according to Eqs. 30–31 for selected values of $j = t/\Delta t$. In some instances, the trajectory was divided into a moderate number of subtrajectories, and $\langle P_2 \rangle$ was computed for each of them. The standard deviation of the values for a given t obtained for the various subtrajectories serves as an estimate of the statistical error of the procedure. This error is expected (23) to decrease with $t/(T - t)$, where T is the length of the simulation, which was always under 0.004. The other possible source of error is the finite value of Δt. To determine whether the above listed values are small enough, calculations for some cases were repeated with a Δt smaller by a factor of five to ten, and increasing the n by the same factor so that T remains unchanged. The $\langle P_2 \rangle$ values were found to be coincident within statistical error.

Before the calculation of the correlation function, a statistical analysis of the trajectory was carried out in all the cases. The distribution of θ was always in agreement with the theoretical Eqs. 10 or 8. The distribution of ϕ was uniform, as it should be. The simulated value of $\langle \cos^2\theta \rangle$ deviated from the theoretical one (Table I) by less than 0.5% for all the simulations.

The simulated correlation functions for the cone model are presented in Fig. 3, where they are compared with the

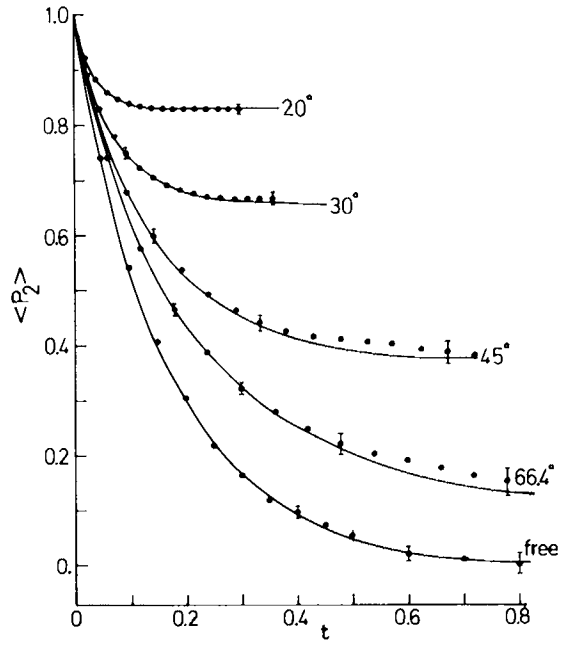

FIGURE 3 $\langle P_2 \rangle$ vs. t for the cone model and free diffusion. (—) and (●) are the theoretical (Eq. 17) and simulation results, respectively. Error bars are statistical uncertainties determined as described in the text.

triple-exponential formula of Lipari and Szabo. Also included are the results for free diffusion. The agreement between the simulated and the theoretical results is very good. Indeed, the theoretical result always falls within one standard deviation of the simulated value. This is a rather conclusive check of the capability of the Brownian dynamics technique to simulate rotational diffusion and confirms the adequacy of the working conditions (values of δ, Δt, and n).

Results were obtained also for the three continuous potentials with the values of the constants listed in Table I. We found that the results for the quadratic potential are practically identical to those for the cosine potential with an equivalent constant (equal S or $\langle P_2 \rangle_\infty$; see Table I) constant. The data in Fig. 1 suggest the reason of this finding. Although $\frac{1}{2}K\theta^2$ and $Q(1 - \cos\theta)$ are quite different from each other when θ exceeds a certain value, the difference is not statistically significant because for both potentials $V \gg kT$ in that region. Thus, the probability functions $p(\theta)$ are nearly coincident, as seen in Fig. 1 *b*.

In Fig. 4 we present some results for the quadratic and squared-sine potentials compared with the theoretical results for the cone model. We note first that for high, equivalent values of the constants ($K = 13.9$ and $C = 8.54$, with the same $\langle P_2 \rangle_\infty$ as $\theta_0 = 30°$) the decays of $\langle P_2 \rangle$ for the two potentials are nearly the same. For high C, in the squared-sine potential the barrier at $\theta_0 = 90°$ is high and its crossing is highly improbable. Thus the particle behaves as if it were confined to one of the two regions, $0 < \theta < 90°$ or $90° < \theta < 180°$. In this region the shape of the $p(\theta)$ function is very similar to that for other potentials, and thus the decays are practically the same. In contrast, the decay for the sine-squared potential with $C = 1.89$ is appreciably faster at long times than that of the quadratic potential with the equivalent constant $K = 2.17$, as seen in Fig. 4. The reason is that by decreasing C height of the barrier decreases, the crossing frequency increases and the orientational relaxation is more rapid.

Fig. 4 also shows that the decays for the continuous potentials are different from those for the cone model. The difference is magnified if one subtracts $\langle P_2 \rangle_\infty$, plotting the decay as $(\langle P_2 \rangle - \langle P_2 \rangle_\infty)/(1 - \langle P_2 \rangle)_\infty$, which goes from 1 for $t = 0$ to 0 for $t \to \infty$ in any case. For the sake of consistency, we use the $\langle P_2 \rangle_\infty$ value calculated from Eqs. 14 and 15 with the result of $\langle \cos^2\theta \rangle$ calculated for the trajectory. Such plots are presented in Fig. 5, using a logarithmic scale to check the possible validity of a monoexponential decay of the form of Eq. 16, for which

$$(\langle P_2 \rangle - \langle P_2 \rangle_\infty)/(1 - \langle P_2 \rangle_\infty) = e^{-t/\sigma}, \qquad (32)$$

where σ is the effective relaxation time (in the notation of references 11–16) and the variation with t in Fig. 5 would be linear. We see that for rather restricted rotation, as is the case for $\theta_0 = 30°$ and the equivalent potentials, the decay is approximately linear down to $\langle P_2 \rangle$ values that are close to $\langle P_2 \rangle_\infty$. σ can be then obtained from the slopes in Fig. 5.

In contrast, for less restricted rotation, the curvature in the cases of the cone model, and the quadratic potential

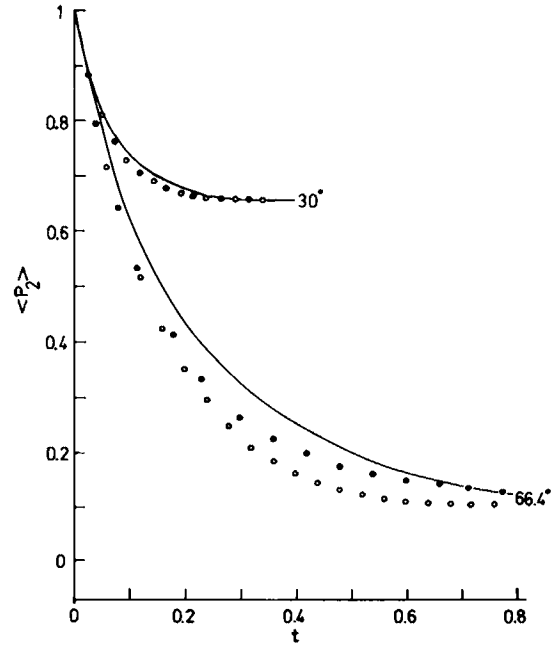

FIGURE 4 Comparison of the decays of $\langle P_2 \rangle$ for the cone model (—), the quadratic potential (●), and the squared-sine potential (○), with $\theta_0 = 30°$, $K = 13.9$, $C = 8.54$ ($\langle P_2 \rangle_\infty = 0.653$), and $\theta_0 = 66.4°$, $K = 2.17$, $C = 1.89$ ($\langle P_2 \rangle_\infty = 0.078$).

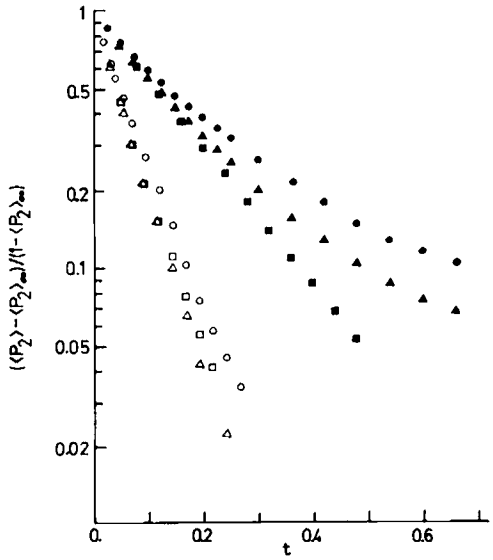

FIGURE 5 Plot of $(\langle P_2 \rangle - \langle P_2 \rangle_\infty)/(1 - \langle P_2 \rangle_\infty)$ vs. t, illustrating the validity of Eq. 32. Circles, triangles, and squares are values for the cone model, quadratic potential, and the squared-sine potential. Open symbols are for $\theta_0 = 30°$, $K = 13.9$, and $C = 8.54$, and closed symbols are for $\theta_0 = 66.4°$, $K = 2.17$, and $C = 1.89$.

suggest a multiexponential decay. However the curvature is not much pronounced. From an experimental point of view, the instrumental noise could blur the curvature and the decay could look linear in the semilogarithmic plot. Therefore, we decided to obtain a σ value for these decays from the straight line that best fits the points in the central part of the decay, chosen as $0.8 \leq (\langle P_2 \rangle - \langle P_2 \rangle_\infty)/(1 - \langle P_2 \rangle_\infty) \leq 0.2$. For the squared-sine potential, we find that the behavior is very linear, i.e., monoexponential, throughout most of the decay. It is interesting to note that the monoexponential approximation, which was introduced to simplify the mathematical treatment of the cone model (12) and the quadratic potential (16), is not rigorously correct for these models, while for the squared-sine potential, which as far as we know has not been considered before, that approximation seems to be essentially correct.

The σ values extracted from Fig. 5 are listed in Table II along with those obtained for the cone model in the monoexponential approximation (Eq. 24 of Lipari and Szabo, reference 12) denoted hereafter as CME. Using these values we can now answer one of the main questions that motivated this study, namely, the error introduced by the CME approximation in the analysis of experimental data.

A practical procedure to analyze experimental data could be as follows: $\langle P_2 \rangle_\infty$ could be obtained from the long-time behavior of the decay curve, or could be calculated from the order parameter, S (Eq. 14), determined by measurements of other properties. Then, one would put $\langle P_2 \rangle$ in the form

$$[(\langle P_2 \rangle - \langle P_2 \rangle_\infty)/(1 - \langle P_2 \rangle_\infty)](t') = e^{-st'}, \tag{33}$$

where

$$s = D_\perp/\sigma. \tag{34}$$

From semilogarithmic plots like those in Fig. 5, one would obtain the slope, s. Alternatively, the variation of $\langle P_2 \rangle$ with t' could be fitted to a single exponential plus baseline, by the nonlinear least-squares method, extracting simultaneously $\langle P_2 \rangle_\infty$ and s. Using Eqs. 10 and 15, $\cos\theta_0$ could be calculated and introduced in the Lipari–Szabo formula to obtain σ_{CME}. Finally the apparent value of the rotational diffusion coefficient would be calculated as

$$D_\perp^{app} = \sigma^{CME} s. \tag{35}$$

Combining Eqs. 34 and 35 we have

$$D_\perp^{app}/D_\perp = \sigma^{CME}/\sigma. \tag{36}$$

Thus, the ratio of the apparent diffusion coefficient to the true one can be estimated from our Brownian dynamics simulation results. The values of $D_\perp^{app}/D_\perp$ are listed in Table II. We see that if the restriction to rotational diffusion were really a cone, $D_\perp^{app}$ would be only a few percent smaller than the true $D_\perp$. Although the CME is particularly erroneous for θ_0 as high as 66.4°, the difference between $D_\perp^{app}$ and $D_\perp$ is only 3% in that case. The reason is that the error in the CME approximation is compensated by the error due to the representation of the decay by straight line plots like Fig. 5.

More realistically, we should assume that the restriction is governed by a continuous potential. Then, our results in Table II indicate that $D_\perp^{app}$ overestimates $D_\perp$ by 20% if the restriction is quite strong. The $D_\perp^{app}/D_\perp$ ratio decreases with the potential constants, goes through a minimum of ~1.10 and increases again. This weak dependence of $D_\perp^{app}/D_\perp$ on the potential constant can be reasonably averaged out, taking $D_\perp^{app}/D_\perp \simeq 1.15$.

As a rule of thumb, we propose that the CME treatment of experimental data produces an overestimation of ~15% in the rotational diffusion coefficient. Perhaps the only exception is for uniaxial systems with a small potential barrier (like the squared-sine potential with low C) for which the overestimation can reach 40%.

A 15% error in $D_\perp$ has little practical significance. Thus, the Lipari–Szabo monoexponential approximation for the cone model can be safely used in the analysis of the experimental decay of fluorescence anisotropy or related properties. This is so despite the fact that the cone model is a strong simplification of any real system, and the monoexponential formula is not its rigorous solution. We have arrived at this conclusion using a Brownian dynamics algorithm to simulate rotational relaxation restricted by different continuous potentials. We have shown that this simulation technique is effective but very simple. If the results reported in this paper for four types of restriction are not sufficient in the interpretation of a particular

TABLE II

σ (IN UNITS OF $D_\perp^{-1}$) OBTAINED FROM PLOTS OF $(\langle P_2 \rangle - \langle P_2 \rangle_\infty)/(1 - \langle P_2 \rangle_\infty)$ VS. t, AND THE RATIO OF THE APPARENT DIFFUSION COEFFICIENT TO THE TRUE ONE

Cone model						$V = \frac{1}{2}K\theta^2$			$V = C\sin^2\theta$		
A_∞	S_2	θ_0	σ	σ_{CME}	$D_\perp^{app}/D_\perp$	K	σ	$D_\perp^{app}/D_\perp$	C	σ	$D_\perp^{app}/D_\perp$
0.830	0.91	20°	0.034	0.0342	1.00	32.2	0.029	1.18	17.5	0.029	1.18
0.653	0.81	30°	0.076	0.0735	0.97	13.9	0.061	1.20	8.54	0.064	1.15
0.364	0.60	45°	0.16	0.146	0.91	5.7	0.13	1.12	4.49	0.13	1.12
0.081	0.28	66.4°	0.24	0.234	0.97	2.17	0.20	1.17	1.89	0.17	1.38

system, the Brownian dynamics technique can be straightforwardly applied to any other complex potential.

This work was supported by Grant 561/84 from the Comision Asesora de Investigación Científica y Técnica to J. G. de la Torre.

Received for publication 29 December 1986 and in final form 20 April 1987.

REFERENCES

1. Belford, G. G., R. L. Belford, and G. Weber. 1972. Dynamics of fluorescence polarization in macromolecules. *Proc. Natl. Acad. Sci. USA.* 69:1392–1393.
2. Ehrenberg, M., and R. Rigler. 1976. Fluorescence correlation spectroscopy applied to rotational diffusion of macromolecules. *Q. Rev. Biophys.* 9:69–79.
3. García de la Torre, J., and V. A. Bloomfield. 1981. Hydrodynamic properties of complex, rigid, biological macromolecules: theory and applications. *Q. Rev. Biophys.* 14:81–139.
4. García de la Torre, J. 1981. Rotational diffusion coefficients. *In* Molecular Electro-optics. S. Krause, editor. Plenum Publishing Corp., New York. 75–103.
5. Jovin, T. M., M. Bartholdi, W. L. C. Vaz, and R. H. Austin. 1981. Rotational diffusion of biological macromolecules by time-resolved delayed luminiscence (phosphorescence, fluorescence) anisotropy. *Ann. NY Acad. Sci.* 366:176–179.
6. Bayley, P. M., and R. E. Dale. 1985. Spectroscopy and the Dynamics of Molecular Biological Systems. Academic Press, Inc., New York. 79–94, 95–108, 119–132.
7. Eads, T. M., D. D. Thomas, and R. H. Austin. 1984. Microsecond rotational motions of eosin-labeled myosin measured by time-resolved anisotropy of absorption and phosphorescence. *J. Mol. Biol.* 179:55–81.
8. Kinosita, K., Jr., S. Ishiwata, H. Yoshimura, H. Asai, and A. Ikegami. 1984. Submicrosecond and microsecond rotational motions of myosin head in solution and in myosin synthetic filaments as revealed by time-resolved optical anisotropy decay measurements. *Biochemistry.* 23:5963–5979.
9. Munro, I., I. Petch, and L. Stryer. 1979. Subnanosecond motions of tryptophan residues in proteins. *Proc. Natl. Acad. Sci. USA.* 76:56–60.
10. Iniesta, A., and García de la Torre. 1987. Rotational diffusion coefficients of a small, spherical subunit flexibly attached to a larger sphere. *Eur. Biophys. J.* In press.
11. Kinosita, K., Jr., S. Kawato, and A. Ikegami. 1977. A theory of fluorescence depolarization decay in membranes. *Biophys. J.* 20:289–305.
12. Lipari, G., and A. Szabo. 1980. Effect of librational motion on fluorescence depolarization and nuclear magnetic resonance relaxation in macromolecules and membranes. *Biophys. J.* 30:489–506.
13. Lipari, G., and A. Szabo. 1981. Padé approximants to correlation functions for restricted rotational diffusion. *J. Chem. Phys.* 75:2971–2976.
14. Szabo, A. 1984. Theory of fluorescence depolarization in macromolecules and membranes. *J. Chem. Phys.* 81:150–167.
15. Fujiwara, T., and K. Nagayama. 1985. The wobbling-in-a-cone analysis of internal motion in macromolecules. *J. Chem. Phys.* 83:3110–3117.
16. Kinosita, K., Jr., A. Ikegami, and S. Kawato. 1982. On the wobbling-in-a-cone analysis of fluorescence anisotropy decay. *Biophys. J.* 37:461–464.
17. Harvey, S. C., and H. Cheung. 1972. Computer simulation of fluorescence depolarization due to Brownian motion. *Proc. Natl. Acad. Sci. USA.* 69:3670–3672.
18. Harvey, S. C., and H. Cheung. 1980. Transport properties of particles with segmental flexibility. II. Decay of fluorescence polarization anisotropy from hinged macromolecules. *Biopolymers.* 19:913–930.
19. Ermak, D. L., and J. A. McCammon. 1978. Brownian dynamics with hydrodynamic interaction. *J. Chem. Phys.* 69:1352–1360.
20. Allison, S. A., and J. A. McCammon. 1984. Transport properties of rigid and flexible macromolecules by Brownian dynamics simulation. *Biopolymers.* 23:167–187.
21. Allison, S. A., and J. A. McCammon. 1984. Multistep Brownian dynamics: application to short wormlike chains. *Biopolymers.* 23:363–375.
22. Allison, S. A. 1986. Brownian dynamics simulation of wormlike chains. Fluorescence depolarization and depolarized light scattering. *Macromolecules.* 19:118–124.
23. Lee, S., and M. Karplus. 1984. Brownian dynamics simulation: statistical error of the correlation functions. *J. Chem. Phys.* 81:6106–6118.
24. García de la Torre, J., and V. Rodes. 1983. Effects from bead size and hydrodynamic interactions on the translational and rotational diffusion coefficients of macromolecular bead models. *J. Chem. Phys.* 79:2454–2460.
25. Rubinstein, R. Y. 1981. Simulation and the Monte Carlo Method. John Wiley & Sons, Inc., New York. 90.